

# A Bayesian Inference Framework for Procedural Material Parameter Estimation

Yu Guo  
University of California,  
Irvine

Milos Hasan  
Adobe Research

Lingqi Yan  
University of California,  
Santa Barbara

Shuang Zhao  
University of California,  
Irvine

## Abstract

*Procedural material models have been gaining traction in many applications thanks to their flexibility, compactness, and easy editability. In this paper, we explore the inverse rendering problem of procedural material parameter estimation from photographs using a Bayesian framework. We use summary functions for comparing unregistered images of a material under known lighting, and we explore both hand-designed and neural summary functions. In addition to estimating the parameters by optimization, we introduce a Bayesian inference approach using Hamiltonian Monte Carlo to sample the space of plausible material parameters, providing additional insight into the structure of the solution space. To demonstrate the effectiveness of our techniques, we fit procedural models of a range of materials—wall plaster, leather, wood, anisotropic brushed metals and metallic paints—to both synthetic and real target images.*

## 1. Introduction

Physically accurate simulation of material appearance is an important yet challenging problem, with applications in many areas from entertainment to product design and architecture visualization. A key ingredient to photorealistic rendering is high-quality material models. Acquiring the parameters of these models from physical measurements (for example, photographs) has been an active research topic in computer vision and graphics.

Recently, *procedural* material models have been gaining significant traction in the industry (e.g., [1]). In contrast to traditional material reflectance models that represent spatially varying surface albedo, roughness, and normal vectors as 2D images, the procedural models generate such infor-

mation using a smaller number of user-facing parameters, providing high compactness and easy editability.

In this paper, we introduce a new differentiable computational framework to estimate the parameters of procedural material models. Our technique enjoys generality by covering a range of materials from standard opaque dielectrics (e.g. plastics, leather, wall paint, wood) to anisotropic brushed metals and metallic paints (Figure 1). Further, we introduce a novel view of the procedural parameter estimation problem in a *Bayesian framework*, precisely defining prior and posterior distributions of the parameters, allowing for both maximization and sampling of the posterior.

The estimation of procedural model parameters faces several challenges. First, the procedural generation (and physics-based rendering) of materials is a complex process with a diverse set of operations, making the relationship between procedural model parameters and properties of the final renderings nonlinear and complicated. Additionally, designing a suitable *loss function* (metric) to compare a synthesized image to a target image is not obvious. This is because the procedurally generated images do not offer pixel-wise alignments to target images, making simple image difference metrics (e.g., L2 or SSIM) unsuitable.

Our contributions lie in the following two main areas. First, we present a general framework to compare simulated and target images in a robust fashion without requiring pixel-wise alignments (§4). To this end, we leverage *summary functions* that map images to latent vectors which can then be compared using L2 or other simple metrics to judge how different two images are. We consider a number of summary functions, from very simple ones (means of fixed image regions), through higher order statistics and Fourier transforms, to neural summary functions (embeddings) based on Gram matrices of VGG feature maps [11, 12]. The neural embedding approach was first introduced to material capture by Aittala et al. [2]; we extend



Figure 1: A scene rendered with material parameters estimated using our method: bumpy dielectrics, leather, plaster, wood, brushed metal, and metallic paint. The insets show a few examples of the initial flash photograph, and our procedural material with parameters found by posterior maximization.

their approach to the case of procedural materials, were it turns out to perform well.

Second, we introduce a *Bayesian inference* approach using Hamiltonian Monte Carlo (HMC) sampling of the space of plausible material parameters (§5). This provides additional information beyond single point estimates of material parameters (for example, though not limited to, discovering similarity structures in the parameter space). Posterior sampling is a well-studied area within statistics but, to our knowledge, has not yet been applied to material appearance acquisition (or inverse rendering in general).

We implement the procedural generation and rendering processes as (differentiable) PyTorch procedures with the priors and summary functions (classical or neural) expressed in the same framework. These four components (priors, procedural material model, rendering, summary function) together define our posterior distribution (outlined in Figure 2), a rather complex (but fully differentiable) function.

To demonstrate the efficacy of our techniques, we fit procedural models of a few materials to both synthetic and real target images (§6).

## 2. Related Work

We review previous work on material parameter estimation in computer graphics and vision, as well as on Hamiltonian Monte Carlo methods in Bayesian inference.

**Per-pixel SVBRDF capture.** A large amount of previous work focuses on acquisition of material data from physical measurements. The methods generally observe the material sample with a fixed camera position, and solve for

the parameters of a spatially-varying BRDF model such as diffuse albedo, roughness (glossiness) and surface normal. They differ in the number of light patterns required and their type; the patterns used include moving linear light [10], Gray code patterns [8] and spherical harmonic illumination [13]. In these approaches, the model and its optimization are specific to the light patterns and the optical setup of the method, as general non-linear optimization was historically deemed inefficient and not robust enough.

More recently, Aittala et al. [3] captured per-pixel SVBRDF data using Fourier patterns projected using an LCD screen; their algorithm used a fairly general, differentiable forward evaluation model, which was inverted in a maximum a-posteriori (MAP) framework. In practice, this was done using a standard non-linear least-squares optimizer with well-chosen priors, showing that a general optimization approach with a differentiable forward model can be successful with carefully chosen illumination patterns, priors and initialization.

Later work by Aittala et al. [4, 2] found per-pixel parameters of stationary spatially-varying SVBRDFs from two-shot and one-shot flash-lit photographs, respectively. In the latter case, the approach used a neural Gram-matrix texture descriptor based on the texture synthesis and feature transfer work of Gatys [11, 12] to compare renderings with similar texture patterns but without pixel alignment. We demonstrate that this descriptor makes an excellent summary function within our framework; in fact, the approach works well in our case, as the procedural nature of the model serves as an additional implicit prior, compared to per-pixel approaches. On the other hand, our forward evaluation process is more complex than Aittala et al., since it also in-

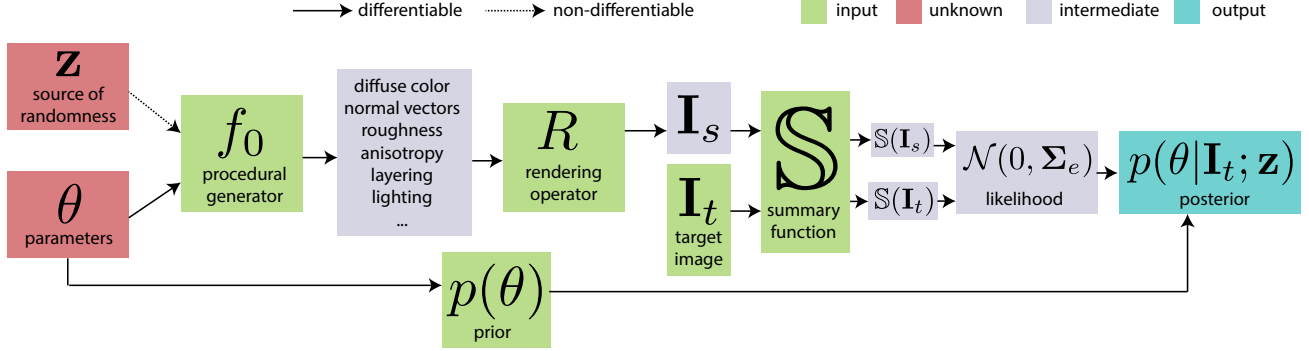


Figure 2: Our differentiable posterior computation combines priors, a procedural material model, a rendering operator, a summary function, and a target image.

cludes the procedural material generation itself.

Recent methods by Deschaintre et al. [7], Li et al. [17] have been able to capture non-stationary SVBRDFs from a single flash photograph by training an end-to-end deep convolutional network. Gao et al. [9] introduced an auto-encoder approach, optimizing the appearance match in the latent space. All of these approaches estimate per-pixel parameters of the microfacet model (diffuse albedo, roughness, normal), and are not obviously applicable to estimation of procedural model parameters, nor to more advanced optical models (significant anisotropy, layering or scattering).

**Procedural material parameter estimation.** Focus on estimating the parameters of procedural models has been relatively rare. The dual-scale glossy parameter estimation work of Wang et al. [23] finds, under step-edge lighting, the parameters of a bumpy surface model consisting of a heightfield constructed from a Gaussian noise power spectrum and global microfacet material parameters. Their results provide impressive accuracy, but the solution is highly specialized for this material model and illumination.

Recently, Hu et al. [14] introduced a method for inverse procedural material modeling that treats the material as a black box, and trains a neural network mapping images to parameter vector predictions. The training data comes from sampling the space of parameters and evaluating the black box model. In our experiments, this approach is less accurate; our fully differentiable models can achieve higher accuracy fits and can be used to explore posterior distributions through sampling.

**Optical parameters of fiber-based models.** Several approaches for rendering of fabrics model the material at the microscopic fiber level [24, 25, 16]. However, the optical properties of the fibers (e.g. roughness, scattering albedo) have to be chosen separately to match real examples. Zhao et al. [24] use a simple but effective trick of matching the

mean and standard deviation (in RGB) of the pixels in a well-chosen area of the target and simulated image. Khurgun et al. [15] have extended this approach with a differentiable volumetric renderer, combined with a stochastic gradient descent; however, their method is still specific to fiber-level modeling of cloth.

**Bayesian inference.** A variety of methods used across the sciences are Bayesian in nature; in this paper, we specifically explore Bayesian inference for parameter estimation through Markov chain Monte Carlo sampling of the posterior distribution. Hamiltonian Monte Carlo (HMC) [19, 5] is an algorithm for sampling a multi-dimensional continuous probability distribution (pdf): given just a piece of code that evaluates the log pdf and its gradient, the method can effectively explore the space, sampling points with probability proportional to the pdf. The gradient information leads to more efficient sampling than simpler methods such as Metropolis-Hastings.

Several software packages exist for Bayesian inference, allowing a user to specify a statistical forward model and parameters. The posterior distribution can then be sampled using HMC or maximized using a non-linear optimizer. An example is STAN [6]. Our earlier version was based on STAN; however, its custom forward models use C++, which we found limiting. We reimplemented key features of Stan (HMC, sigmoid transforms of parameters) in PyTorch, which gave our system higher flexibility and extensibility.

### 3. Preliminaries

**Procedural model generation.** We focus on *procedural material models* which utilize specialized operators to generate spatially varying surface reflectance profiles. Specifically, let  $\theta$  be the parameters taken by some procedural material generation process  $f_0$ . Then,  $f_0(\theta)$  generates the material properties (e.g., albedo, roughness, surface normals, anisotropy, scattering, etc.), in addition to any other param-

eters required by rendering (e.g. light parameters), which can in turn be converted into a rendered image  $I_s$  via the standard rendering process  $R$ . This *forward evaluation* process can be summarized as

$$I_s = R(f_0(\theta)) = f(\theta), \quad (1)$$

where  $f$  is the composition of  $R$  and  $f_0$ .

When modeling real-world materials, it is desirable to capture naturally arising irregularities. In procedural modeling, this is usually achieved by making the model generation process  $f_0$  to take extra random input  $z$  (e.g., random seeds, pre-generated noise textures, etc.) that is then used to create the irregularities. This also causes the full forward evaluation to become  $f(\theta; z) := R(f_0(\theta; z))$ .

**Inverse problem specification.** We consider the problem of inferring procedural model parameters  $\theta$  given a target image  $I_t$  (which is typically a photograph of a material sample under known illumination). This, essentially, requires inverting  $f$  in Eq. (1):  $\theta = f^{-1}(I_t)$ . Direct inversion of  $f = R \circ f_0$  is intractable for any but the simplest material and rendering models. Instead, we aim to find  $\theta$  such that  $I_s$  has similar appearance to  $I_t$ :

$$\text{find } \theta \text{ s.t. } I_t \approx f(\theta; z), \quad (2)$$

for some (any)  $z$ , where  $\approx$  is an *appearance-match* relation that will be discussed in the next section.

## 4. Summary Functions

To solve the parameter estimation problem using Eq. (2), a key ingredient is the appearance-match relation. Unfortunately, we cannot use simplistic image difference metrics such as the L2 or L1 norms. This is because the features (bumps, scratches, flakes, yarns, etc.) in the images of real-world materials are generally misaligned, even when the two images represent the same material. In procedural modeling, as shown in Figure 3, with irregularities created differently using  $z_1$  and  $z_2$ , the same procedural model parameters  $\theta$  can yield slightly different results  $f(\theta; z_1)$  and  $f(\theta; z_2)$ .

To address this challenge, we introduce a *summary function*, which abstracts away the unimportant differences in the placement of the features, and summarizes the predicted and target images into smaller vectors whose similarity can be judged with simple metrics like L2 distance.

An image summary function (embedding)  $\mathbb{S}$  is a continuous function that maps an image of a material ( $I_t$  or  $I_s$ ) into a vector in  $\mathbb{R}^k$ . An idealized summary function would have the property that

$$\mathbb{S}(f(\theta_1, z_1)) = \mathbb{S}(f(\theta_2, z_2)) \Leftrightarrow \theta_1 = \theta_2. \quad (3)$$

That is, applying the summary function would fully abstract away from the randomness  $z$  and the difference between

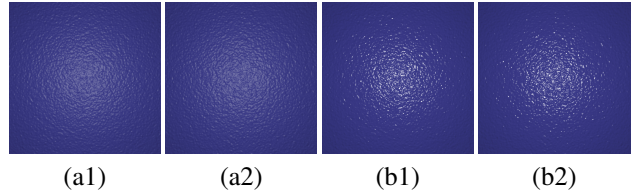


Figure 3: Each pair of images among (a, b) are generated using identical model parameters  $\theta$  but different irregularities  $z$ . The pixel-wise L2 norm of the difference between these image pairs is large and not useful for estimating model parameters.

the two summary vectors would be entirely due to different material properties  $\theta$ .

Practical summary functions will satisfy the above only approximately. However, a good practical summary function will embed images of the same material close to each other, and images of different materials further away from each other. Below we discuss several techniques for constructing summary functions.

### 4.1. Our Summary Functions

**Statistics of image bins.** The simplest idea for a summary function is to subdivide the image into  $k$  bins (regions) and compute the (scalar or RGB) mean of each region. For mostly isotropic materials, a flash photograph will normally lead to an approximately radially symmetric highlight, where we found concentric bins perform well. For anisotropic highlights (e.g. brushed metal), it makes more sense to define the bins as  $k$  vertical or horizontal bands. Adding the standard deviation statistic per bin, in addition to mean, can significantly help with estimating frequencies and size of features such as bumps.

**Fourier transforms.** However, the simple per-bin statistics can be insufficient to precisely match frequency characteristics of material imperfections. A more complex and more powerful tool for summary function design is fast Fourier transforms, which captures frequencies explicitly. These can be applied to the whole image (as a 2D FFT), or part of it, e.g. as 1D FFTs over a subset of rows or columns. Note that automatic computation of derivatives is possible with the FFT, and supported by the PyTorch framework.

**Neural summary function.** Gatys et al. [11, 12] introduced the idea of using the features of an image classification neural network (usually VGG [21]) as a descriptor  $T_G$  of image texture (or style). Optimizing images to minimize the difference in  $T_G$  (combined with other constraints) allowed Gatys et al. to produce impressive, state-of-the-art results for parametric texture synthesis and style transfer between images. While further work has introduced improve-

ments [20], we find that the original version from Gatys et al. works already well in our case.

Aittala et al. [2] introduced this idea to capturing material parameter textures (albedo, roughness, normal and specular maps) of stationary materials. They optimized for a  $256 \times 256$  stationary patch that matches the target image in various crops, using a combination of  $T_G$  and a number of special Fourier-domain priors. In our case (for procedural materials), we find that the neural summary function  $T_G$  works even more effectively; we can simply apply it to the entire target or simulated images (not requiring crops nor Fourier-domain priors). Specifically, define the Gram matrix  $G$  of a set of feature maps  $F_1, \dots, F_n$  as

$$G = \text{mean}(F_i \cdot F_j), \quad (4)$$

where the product  $F_i \cdot F_j$  is element-wise.  $T_G$  is defined as the concatenation of the flattened Gram matrices computed for the feature maps before each pooling operation in VGG19. Note that the size of the Gram matrices depends on the number of feature maps (channels), not their size; thus  $T_G$  is independent of input image size.

## 5. Bayesian Inference

In what follows, we first summarize the classical non-linear optimization approach to parameter estimation (and inverse problems in general), and its Bayesian formulation as a maximum a-posteriori (MAP) estimate. These approaches generally provide a reasonable single point estimate of the parameter vector. Next, we explain how the Hamiltonian Monte Carlo approach for Bayesian inference extends the classical approach.

### 5.1. Point Estimates

**Non-linear optimization.** Recall that our goal is to match the target  $I_t$ , normally an image of a material sample under known illumination conditions. The model has unknown parameters  $\theta$ . The *forward evaluator*  $f(\theta, z)$  is available as a differentiable subroutine. Given the availability of an appropriate summary function  $\mathbb{S}$ , our goal is to find the value of  $\theta$  whose summary vector fits that of the target (measurement)  $I_t$  as closely as possible:

$$\arg \min_{\theta} \|\mathbb{S}(f(\theta, z)) - \mathbb{S}(I_t)\|^2. \quad (5)$$

Recall that we are generally not interested in estimating  $z$  that is meant to introduce irregularities. The optimization in Eq. (5) can be solved by standard non-linear optimization methods; regularization is commonly added to improve the stability.

**Maximum a-posteriori estimation.** A technically similar but theoretically cleaner approach is to model the above in a probabilistic Bayesian framework, as the maximization

of the posterior distribution. We treat the procedural model parameters  $\theta$  as random variables with corresponding probability distributions.

Specifically, we introduce a *prior* probability distribution  $p(\theta)$  of the parameters, reflecting our pre-existing beliefs about the likelihood values of the unknown parameters. For example, in most material models, we know what range the albedo color and roughness coefficients of the material should typically be in.

Further, we model the  $\approx$  operator from Eq. (2) as an error distribution. Precisely, we postulate that the difference between the simulated image summary  $\mathbb{S}(f(\theta, z))$  and the target image summary  $\mathbb{S}(I_t)$  follows a known probability distribution. In practice, we use a (multi-variate) normal distribution with zero mean and the covariance  $\Sigma_e$ :

$$\mathbb{S}(f(\theta, z)) - \mathbb{S}(I_t) \sim \mathcal{N}(0, \Sigma_e). \quad (6)$$

Our experiments indicate that this simple error distribution works well in practice, and we regard  $\Sigma_e$  as a hyperparameter and set it manually.

We also have multiple options in handling the random vector  $z$ . While it is certainly theoretically possible to estimate it, we are not really interested in its values; we find it simpler and more efficient to simply choose  $z$  randomly, fix it, and assume it known during the process of estimating the “interesting” parameters  $\theta$ .

Under these assumptions, according to the Bayes theorem, we can write down the posterior probability of parameters  $\theta$ , conditional on the known values of  $I_t$  and  $z$ , as:

$$p(\theta|I_t, z) \propto \mathcal{N}[\mathbb{S}(f(\theta, z)) - \mathbb{S}(I_t); 0, \Sigma_e] p(\theta), \quad (7)$$

where the right side does not need to be normalized. For numerical stability, we compute the negative log posterior, viz.  $-\log p(\theta|I_t, z)$ , in practice.

In the maximum a-posteriori (MAP) framework we estimate the desired parameter values  $\theta$  as the maximum of the posterior pdf  $p(\theta|I_t, z)$  given by Eq. (7). This problem can be solved using many non-linear optimization algorithms.

### 5.2. Monte Carlo Sampling of the Posterior

Although the point estimate approach gives satisfactory results in many cases, it is not without problems. For example, since a perfect match between a procedural material and a photograph is generally impossible, it can be desired to have a set of imperfect matches for the user to choose from. Further, there could be an entire subset of the parameter space giving solutions of approximately equivalent fit under the target view and lighting; however, these may look quite different from each other in other configurations, and a user may want to explore those differences.

In this paper, we use the well-known technique of full Bayesian inference, sampling the posterior pdf defined

in Eq. (7) using Markov-chain Monte Carlo techniques, specifically Hamiltonian Monte Carlo (HMC) [5]. While well explored in statistics and various scientific fields, to our knowledge, this technique has not been used for the inference of material parameters.

The goal of the sampling is to explore the posterior with many (typically thousands or more) samples, each of which represents a material parameter vector consistent with the target image. Plotting these samples projected into two dimensions (for a given pair of parameters) gives valuable insight into similarity structures. Furthermore, interactively clicking on samples and observing the predicted result can help a user to quickly zoom in on a preferred solution, which an automatic optimization algorithm is fundamentally incapable of.

Technically, HMC is similar to other Markov chain methods such as Metropolis-Hastings but is much more efficient for posterior sampling problems in cases where the derivatives of the model are available (always true in our case, as all our forward evaluators are implemented in PyTorch).

## 6. Material Models and Results

We now demonstrate the effectiveness of our technique by fitting six procedural material models—bumpy microfacet surface, brushed metal, metallic paint with flakes, leather, plaster, and wood—to a mix of synthetic and real target images. We also show a translucent material in the supplementary material.

Our forward evaluation process has the camera and light co-located. This configuration closely matches a mobile phone camera with flash (which is what we use to take the real target images) and simplifies some BRDF formulations (because the incoming, outgoing, and half-way vectors are all identical). Further, we assume that the distance between camera and sample is known as it is generally easy to measure or estimate. The knowledge of the camera field of view allows us to compute the physical scale of the resulting pixels. Lastly, we treat light intensity and vignetting (expressed as an image-space Gaussian function) as (unknown) parameters of the forward evaluation process so that they do not need to be calibrated.

All the procedural material models we used, which will be detailed in §6.1, are implemented using PyTorch which automatically provides GPU acceleration and computes derivatives through backpropagation. For all material parameter inference tasks, our forward evaluation generates  $256 \times 256$  images. Notice that the recovered parameters can then be used to generate results with much higher resolution because the procedural models are generally resolution-independent.

We show results generated using six synthetic images in Figure 4 and four real photographs (taken with an iPhone 7)

Table 1: Performance statistics for our optimization-based point estimate as well as HMC-based posterior sampling. The numbers are collected by drawing 20k samples using a workstation equipped with an Intel i7-6800K six-core CPU and an Nvidia GTX 1080 GPU. The optimization involves one forward evaluation (and backpropagation) per iteration; while the HMC takes ten per sample on average<sup>1</sup>.

Material	# params	Optim. (1k samples)	HMC (1k iter.)
Bump	8	45 s	350 s
Leather	10	50 s	415 s
Plaster	10	50 s	390 s
Flakes	13	50 s	400 s
Metal	10	45 s	380 s
Wood	23	265 s	1960 s

in Figure 5. Please see the supplemental material for more results, including animations illustrating the optimization and sampling progress.

### 6.1. Procedural Material Models

We now describe six procedural models tested. Please refer to the supplement for their PyTorch implementation.

**Bumpy microfacet surface.** This model depicts an opaque dielectric surface with an isotropic noise heightfield. We use a standard microfacet BRDF with the GGX normal distribution [22] combined with a normal map computed from an explicitly constructed heightfield. We assume that the Fresnel reflectance at normal incidence can be computed from a known index of refraction (a value of 1.5 is a good estimate for plastics). We assume an unknown roughness  $r$  (GGX parameter  $\alpha = r^2$ ) and a Lambertian diffuse term with unknown albedo  $\rho$ . This model is identical to Wang et al. [23], except using the GGX instead of Beckmann microfacet distribution. The main practical difference from the capture setup in that paper is that we use a point light, instead of step-edge illumination.

The bumpy heightfield is constructed using an inverse Fourier process including: (i) choosing a power spectrum in the continuous Fourier domain; (ii) discretizing it onto a grid of complex numbers; (iii) randomly choosing the phase of each texel on the grid (while keeping the chosen amplitude); and (iv) applying an inverse fast Fourier transform whose real component becomes the resulting heightfield. At render time, we use the normal map derived from this heightfield.

<sup>1</sup>In HMC sampling, each sample needs  $(s + 3)/r$  forward evaluations on average where  $s$  indicates the number of leapfrog steps and  $r$  denotes the acceptance rate. In practice, we set  $s = 4$  and have  $r = 70\%$ , causing the expected number of evaluations per sample to be 10.

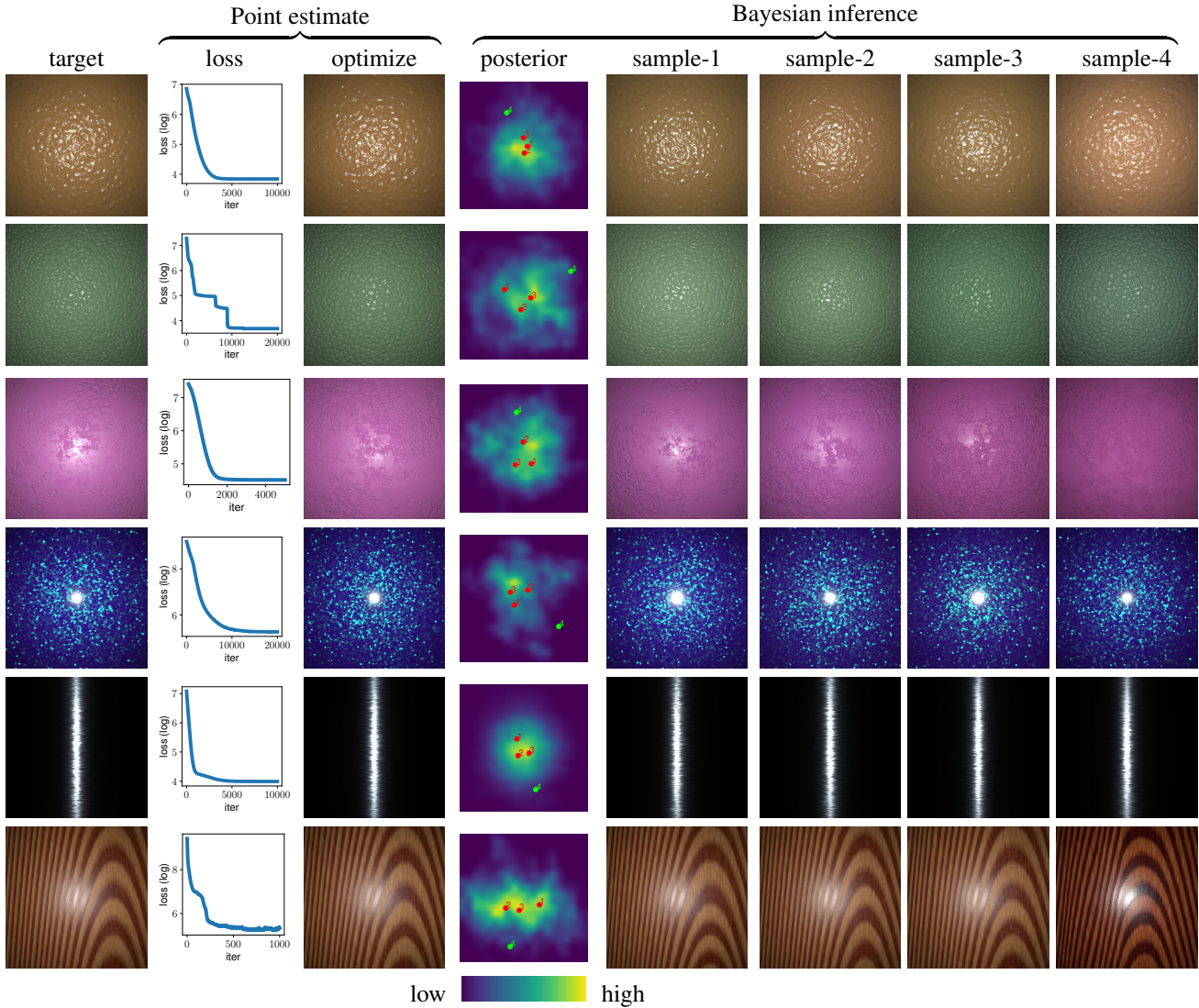


Figure 4: **Optimization and HMC sampling on synthetic images.** Each row corresponds to a different material. From top: bump, leather, plaster, metallic flake, brushed metal and wood. Column 1 is rendered images using different forward models. We show optimization results in columns 2 and 3, samplings in the rest columns. For high dimensional posterior visualization, we project them to 2D using PCA. Here we only show the first two major components. The three red dots corresponding to sample-1,2,3, which are closer to the peak of high dimensional distribution. and the green dot (sample-4) is the opposite. More results please refer to supplemental materials.

**Leather and plaster.** These materials can be modeled similarly as the aforementioned bumpy surfaces except for the computation of the heightfield and roughness. For plaster, a fractal noise texture is scaled (in space and intensity) and thresholded (controlled by additional parameters) to produce both the heightfield and a roughness variation texture. For leather, on the contrary, a Voronoi cell map is used to get the effect of leather-like cells (with parameters for scaling and thresholding), and additional small-scale fractal noise is added.

**Brushed metal.** The brushed metal material extends the above bumpy surface, by introducing anisotropy to both the GGX normal distribution and the noise heightfield used to compute the normal map, while dropping the diffuse term. We make both the BRDF and the Fourier-domain Gaussian power spectrum anisotropic. The parameters of the model thus include two roughnesses, as well as two Fourier-domain standard deviations. We make the anisotropic highlight vertical and centered in the target image.

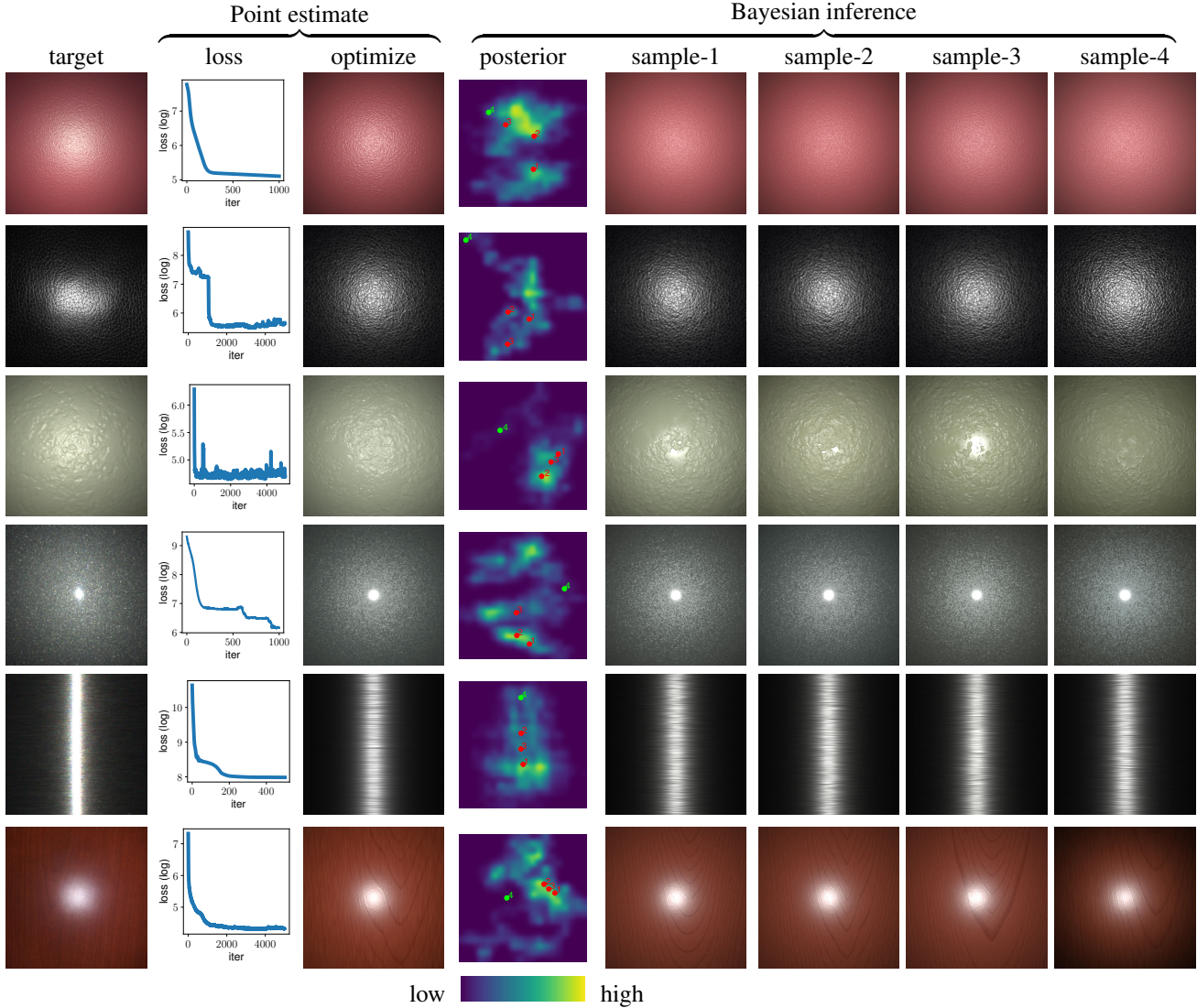


Figure 5: **Optimization and HMC sampling on real photos.** Each row corresponds to a different material. From top: bump, leather, plaster, metallic flake, brushed metal and wood. Similar to Figure 4, except column 1 here contains real photos, columns 2 and 3 show point estimates (via non-linear optimization), and the remaining columns show HMC sampling results. Please refer to the supplemental material to see more results.

**Metallic flakes.** Metallic paint with flakes is a stochastic material with multiple BRDF lobes (caused by light reflecting off the flakes). Our model involves three components, each being an isotropic microfacet lobe, to describe top coating, flakes and glow, respectively. The top coating is usually highly specular, and we make its roughness a model parameter. We assume an index of refraction of 1.5, implying a Fresnel (Schlick) reflectivity at normal incidence of 0.04. The flakes are chosen as Voronoi cells of a random blue-noise point distribution; they have a roughness parameter and varying normals chosen from the Beckmann distribution with an unknown roughness, and with unknown

Fresnel reflectivity. The scale of the cell map is itself a (differentiable) parameter. Lastly, the glow is a component approximating the internal scattering between the top interface and the flakes, and has its own roughness, Fresnel reflectivity and a flat normal. An extra weight parameter linearly combines the flakes and the glow.

**Wood.** Lastly, we created a partial PyTorch implementation of the comprehensive 3D wood model of Liu et al. [18]. This material is a 3D model of the growth rings of a tree, with a number of parameters controlling colors and widths of growth rings, as well as global distortions and small-scale



noise features. We do not implement pores or anisotropic fiber highlights. The 3D wood is finally projected by a cutting plane to image space, defining diffuse albedo, roughness and height.

## 7. Conclusion

Procedural material models have become increasingly more popular in the industry, thanks to their flexibility, compactness, as well as easy editability. In this paper, we introduced a new computational framework to solve the inverse problem: the inference of procedural model parameters based on a single input image.

The first major ingredient to our technique is a family of *summary functions*, from hand-crafted to neural-network based [11, 2], that enable robust calculation of image differences (without requiring pixel-level alignments). The second ingredient is a *Bayesian inference method* that leverages Hamiltonian Monte Carlo (HMC) to sample posterior distributions of procedural material parameters. This technique provides users additional information beyond single point estimates and, to our knowledge, has previously not been applied to inverse-rendering problems.

In the future, we would like to increase the complexity of the models supported even further, to handle materials like woven fabrics, transmissive BTDFs, and more.

## References

- [1] Adobe. Substance, 2019. [www.substance3d.com](http://www.substance3d.com). 1
- [2] Miika Aittala, Timo Aila, and Jaakko Lehtinen. Reflectance modeling by neural texture synthesis. *ACM Trans. Graph.*, 35(4):65:1–65:13, 2016. 1, 2, 5, 9
- [3] Miika Aittala, Tim Weyrich, and Jaakko Lehtinen. Practical svbrdf capture in the frequency domain. *ACM Trans. Graph.*, 32(4):110:1–110:12, July 2013. 2
- [4] Miika Aittala, Tim Weyrich, and Jaakko Lehtinen. Two-shot svbrdf capture for stationary materials. *ACM Trans. Graph.*, 34(4):110:1–110:13, July 2015. 2
- [5] Michael Betancourt. A conceptual introduction to hamiltonian monte carlo, 2017. [arxiv:1701.02434](https://arxiv.org/abs/1701.02434). 3, 6
- [6] Bob Carpenter, Andrew Gelman, Matthew Hoffman, Daniel Lee, Ben Goodrich, Michael Betancourt, Marcus Brubaker, Jiqiang Guo, Peter Li, and Allen Riddell. Stan: A probabilistic programming language. *Journal of Statistical Software, Articles*, 76(1):1–32, 2017. 3
- [7] Valentin Deschaintre, Miika Aittala, Fredo Durand, George Drettakis, and Adrien Bousseau. Single-image svbrdf capture with a rendering-aware deep network. *ACM Trans. Graph.*, 37(4):128:1–128:15, July 2018. 3
- [8] Yannick Francken, Tom Cuyppers, Tom Mertens, and Philippe Bekaert. Gloss and normal map acquisition of mesostructures using gray codes. In *Advances in Visual Computing, 5th International Symposium, ISVC 2009, Las Vegas, NV, USA, November 30 - December 2, 2009, Proceedings, Part II*, volume 5876 of *Lecture Notes in Computer Science*, pages 788–798. Springer, 2009. 2
- [9] Duan Gao, Xiao Li, Yue Dong, Pieter Peers, Kun Xu, and Xin Tong. Deep inverse rendering for high-resolution SVBRDF estimation from an arbitrary number of images. *ACM Trans. Graph.*, 38(4):134:1–134:15, July 2019. 3
- [10] Andrew Gardner, Chris Tchou, Tim Hawkins, and Paul Debevec. Linear light source reflectometry. *ACM Trans. Graph.*, 22(3):749–758, July 2003. 2
- [11] Leon A. Gatys, Alexander S. Ecker, and Matthias Bethge. A neural algorithm of artistic style, 2015. 1, 2, 4, 9
- [12] L. A. Gatys, A. S. Ecker, and M. Bethge. Image style transfer using convolutional neural networks. In *2016 IEEE Conference on Computer Vision and Pattern Recognition (CVPR)*, pages 2414–2423, June 2016. 1, 2, 4
- [13] Abhijeet Ghosh, Tongbo Chen, Pieter Peers, Cyrus A. Wilson, and Paul Debevec. Estimating specular roughness and anisotropy from second order spherical gradient illumination. In *Proceedings of the Twentieth Eurographics Conference on Rendering, EGSR'09*, pages 1161–1170, 2009. 2
- [14] Yiwei Hu, Julie Dorsey, and Holly Rushmeier. A novel framework for inverse procedural texture modeling. *ACM Trans. Graph.*, 38(6):186:1–186:14, Nov. 2019. 3
- [15] Pramook Khungurn, Daniel Schroeder, Shuang Zhao, Kavita Bala, and Steve Marschner. Matching real fabrics with micro-appearance models. *ACM Trans. Graph.*, 35(1):1:1–1:26, Dec. 2015. 3
- [16] Jonathan Leaf, Rundong Wu, Eston Schweickart, Doug L. James, and Steve Marschner. Interactive design of periodic yarn-level cloth patterns. *ACM Trans. Graph.*, 37(6):202:1–202:15, Dec. 2018. 3
- [17] Zhengqin Li, Kalyan Sunkavalli, and Manmohan Chandraker. Materials for masses: SVBRDF acquisition with a single mobile phone image. In *Computer Vision - ECCV 2018 - 15th European Conference, Munich, Germany, September 8-14, 2018, Proceedings, Part III*, volume 11207 of *Lecture Notes in Computer Science*, pages 74–90, 2018. 3
- [18] Albert Julius Liu, Zhao Dong, Miloš Hašan, and Steve Marschner. Simulating the structure and texture of solid wood. *ACM Trans. Graph.*, 35(6):170:1–170:11, Nov. 2016. 8
- [19] Radford M. Neal. MCMC using Hamiltonian dynamics. *arXiv e-prints*, page arXiv:1206.1901, Jun 2012. 3
- [20] Eric Risser, Pierre Wilmot, and Connelly Barnes. Stable and controllable neural texture synthesis and style transfer using histogram losses, 2017. 5
- [21] Karen Simonyan and Andrew Zisserman. Very deep convolutional networks for large-scale image recognition. In *International Conference on Learning Representations*, 2015. 4
- [22] Bruce Walter, Stephen R. Marschner, Hongsong Li, and Kenneth E. Torrance. Microfacet models for refraction through rough surfaces. *EGSR 07*, pages 195–206, 2007. 6
- [23] Chun-Po Wang, Noah Snavely, and Steve Marschner. Estimating dual-scale properties of glossy surfaces from step-edge lighting. In *Proceedings of the 2011 SIGGRAPH Asia Conference, SA '11*, pages 172:1–172:12, 2011. 3, 6
- [24] Shuang Zhao, Wenzel Jakob, Steve Marschner, and Kavita Bala. Building volumetric appearance models of fabric using

micro ct imaging. *ACM Trans. Graph.*, 30(4):44:1–44:10, July 2011. 3

- [25] Shuang Zhao, Fujun Luan, and Kavita Bala. Fitting procedural yarn models for realistic cloth rendering. *ACM Trans. Graph.*, 35(4):51:1–51:11, July 2016. 3